Closed-Form Joint Symbol and Channel Estimation in Hybrid-RIS-aided Communication Systems

Amarilton L. Magalhães*†, Gilderlan T. de Araújo*†, Fazal-E-Asim† and André L. F. de Almeida†

Federal University of Ceara, Brazil†, Federal Institute of Education, Science and Technology of Ceara, Brazil*
e-mail: {amarilton,gilderlan,fazalasim,andre}@gtel.ufc.br

***Abstract*— In this work, we explore a hybrid reconfigurable intelligent surface (HRIS) where the metasurface elements can sense a fraction of the incoming signals while enabling baseband signal processing in the digital domain when the elements are linked to the controller via radio-frequency chains. We consider a single-user, multiple-input multiple-output system where the channel between the user terminal (UT) and HRIS experiences short-term changes due to UT mobility. By capitalizing on a tensor modeling approach, we propose a closed-form semi-blind receiver for the HRIS controller to estimate channels and symbols jointly without relying solely on training sequences. Simulation results show the robustness of our proposed closed-form semi-blind receiver in estimating the time-varying UT-HRIS channel while decoding the transmitted symbols.**

***Keywords*— RIS, HRIS, channel estimation, tensor modeling, semi-blind estimation.**

I. Introduction

Reconfigurable intelligent surface (RIS) is an attractive solution for enhancing future wireless communication networks due to its promising ability to shape the wireless propagation environment [1]. RIS comprises numerous passive reflective elements arranged on a flat surface, where each element can independently modify the phase of the impinging electromagnetic waves [2]. To design the RIS reflection coefficients, the precoder/beamformer at the base station (BS) and the user terminal (UT), obtaining accurate channel state information (CSI) is required. However, this task is hard in RIS-assisted wireless communication systems [3], [4], [5]. In particular, for applications such as mobility tracking, channel sounding, and user localization, an ambiguity-free separate channel estimation (CE) is desirable [6], [7]. In addition, some precoding designs depend on the availability of the individual channels, as discussed in [8]. Supplementary methods are needed to obtain such separate estimates of the involved channels from the cascaded one. One solution is to upgrade the RIS hardware architecture to enable additional signal processing features [9]. Focusing on hardware modification, emerging hybrid RIS architectures have related in recent publications [10], [11], [9], [12]. A comprehensive study about various hybrid architectures can be found in [13].

The authors acknowledge the support of Fundação Cearense de Apoio ao Desenvolvimento Científico e Tecnológico (FUNCAP) under grants FC3-00198-00056.01.00/22, UNI-0210-00043.01.00/23, ITR-0214-00041.01.00/23, the National Institute of Science and Technology (INCT-Signals) sponsored by CNPq under grant 406517/2022-3, and the Coordenação de Aperfeiçoamento de Pessoal de Nível Superior - Brazil (CAPES) - Finance Code 001. This work is also partially supported by CNPq under grants 312491/2020-4 and 443272/2023-9.

Tensor decompositions have been widely used to model wireless communications while providing powerful solutions to solve joint channel and symbol estimation in single- and multiple-antenna systems [14], [15], [16], [17]. Recently, tensor signal processing has been used in the context of RIS-aided communication systems [18], [19], [20], [21]. Such studies have emphasized the effectiveness of tensor-based receivers in providing decoupled estimates of the UT-RIS and RIS-BS channels [18] under more flexible system setups. Recent works [20], [21] have also shown derived (semi)-blind receivers for RIS-assisted multiple-input multiple-output (MIMO) communications, which combine channel and symbol estimation using iterative and closed-form methods. However, the aforementioned works assume a passive RIS architecture, where signal processing only occurs at the receiver.

In this work, we explore the so-called hybrid RIS architecture proposed in [12], which is composed of elements able to sense a fraction of the incoming signal while reflecting the rest. We refer to this architecture simply as hybrid RIS (HRIS). The sensing capability of the HRIS enables baseband signal processing in the digital domain when the elements are linked to its controller via radio frequency (RF) chains. Capitalizing on a tensor modeling approach, we formulate a closed-form semi-blind receiver for the HRIS controller's side to jointly estimate the uplink UT-HRIS channels and symbols involved in a single-user MIMO system. Such estimates are conveyed *via* control link from HRIS to BS to allow an estimation of the HRIS-BS channel through solving a simple least-squares (LS) problem. Avoiding dedicated training sequences for CE, our method enables the HRIS digital controller to estimate several short-term variations of the UT-HRIS channel in a scenario under a certain UT mobility. In addition, such sequential versions of the UT-HRIS channel may be useful for the BS (or even the HRIS) to feed user tracking algorithms and to predict its next position to obtain a more accurate CSI.

A. Notations and Tensor Preliminaries

Scalars, vectors, matrices, and tensors are denoted by lowercase a, bold lowercase $\boldsymbol{a}$, bold uppercase $\mathbf{A}$, and calligraphic $\mathcal{A}$ letters, respectively. The Moore-Penrose pseudo-inverse and the transpose of $\mathbf{A}$ are indicated as $\mathbf{A}^{\mathrm{T}}$ and $\mathbf{A}^{\dagger}$. The symbol $\otimes$ denotes the Kronecker matrix product, and $||\cdot||_{\mathrm{F}}$ is the Frobenius norm. Stated $\mathbf{A} \in \mathbb{C}^{I \times J}$, the vectorization operation $\mathrm{vec}\{\mathbf{A}\}$ outputs the vector $\boldsymbol{a} \in \mathbb{C}^{JI \times 1}$, and the reverse operation $\mathrm{unvec}_{I \times J}(\boldsymbol{a})$ returns $\mathbf{A}$. In addition, $\mathrm{diag}\{\boldsymbol{a}\}$ is the

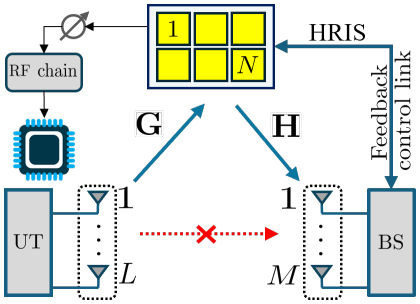

Fig. 1. HRIS-assisted MIMO system model.

diagonal matrix created from $\boldsymbol{a}$. A tensor $\mathcal{A} \in \mathbb{C}^{I_1 \times I_2 \times \cdots \times I_P}$ is referred to as a multidimensional array with order P, and unfolding involves reshaping such a tensor into a matrix. For example, consider a 4-th order tensor $\mathcal{A}$. For instance, the mode-1 and mode-4 unfoldings of $\mathcal{A}$ are denoted by $[\mathcal{A}]_{(2)} \in \mathbb{C}^{I_2 \times I_4 I_3 I_1}$ and $[\mathcal{A}]_{(4)} \in \mathbb{C}^{I_4 \times I_3 I_2 I_1}$, respectively. Beyond the mode-n unfoldings, we can construct generalized matrix unfoldings of $\mathcal{A}$ by considering two on-overlapping subsets of any of the P dimensions, in which the first subset has cardinality Q while the second has $P - Q$ [22]. For instance, $[\mathcal{A}]_{([1,3],[2,4])} \in \mathbb{C}^{I_3 I_1 \times I_4 I_2}$ denotes the generalized unfolding of $\mathcal{A}$ in which the mode 1 and mode 3 vary along the rows while the mode 2 and mode 4 along the columns. In addition, mode 1 exhibits the fastest variation among the rows, and mode 4 varies the fastest among the columns. Note that the mode-n unfolding is a particular case whose single variation among the rows is dictated by the mode n.

II. System Model

We consider an HRIS-aided MIMO wireless communication system, illustrated in Fig. 1, which is composed of one UT and BS equipped with L and M antennas, respectively. Considering a blockage in the direct link, the HRIS comprised of N elements and N_c RF chains [12] assists the communication between UT and BS in an uplink direction. Perfect control feedback link between BS and HRIS is assumed [23]. Since a fraction of the incoming wave is coupled to the sampling waveguide, the power splitting parameter $\rho_{n,t} \in [0, 1]$ indicates the portion of the signal reflected from the n-th HRIS element at the t-th instant with a reconfigurable reflecting phase-shift $e^{j\psi_{n,t}}$. Hence, the remainder portion $1 - \rho_{n,t}$ is sensed and forwarded to the controller through RF chains *via* analog combining. In this sense, $e^{j\phi_{n_c,n,t}}$ is the reconfigurable sensing phase-shift related to the n_c-th RF chain.

We consider a transmission scheme in which the symbols are time spread across I sub-frames, each composed of K blocks of T symbol periods each. Assuming that the BS and HRIS are located in fixed positions, the HRIS-BS channel can be considered to remain constant over the I sub-frames, following a quasi-static regime [24], [19] since its changing is much slower than the UT-HRIS one. In contrast, we assume that the UT-HRIS channel may vary from one sub-frame to another due to the UT mobility such that its i-th version remains unchanged within the i-th sub-frame ($i = 1, \cdots, I$).

Prior to transmission, at the t-th symbol period ($t = 1, \cdots, T$) of the k-th block ($k = 1, \cdots, K$), the UT symbols $\boldsymbol{x}_t = [x_{1,t}, \cdots, x_{R,t}]^{\mathrm{T}} \in \mathbb{C}^{R \times 1}$ are coded following a tensor space-time coding scheme to produce $\boldsymbol{s}_{t,k} = \mathbf{C}_k \boldsymbol{x}_t \in \mathbb{C}^{L \times 1}$, where the coding matrix $\mathbf{C}_k \in \mathbb{C}^{L \times R}$ is the k-th slice of the coding tensor $\mathcal{C} \in \mathbb{C}^{L \times R \times K}$. We assume that the coding matrix is constant within the k-th block and varies from one block to another, which implies $\mathbf{C}_{t,k} = \mathbf{C}_k$. The same assumption stems for the HRIS parameters $\rho_{n,k}$, $\psi_{n,k}$, and $\phi_{n_c,n,k}$. The fraction of the transmitted signal, which is sensed by the N elements and conveyed to the N_c RF chains *via* analog combining, is given by

$$\boldsymbol{y}^{\mathrm{RC}}_{t,k,i} = \boldsymbol{\Phi}_k \mathbf{G}_i \mathbf{C}_k \boldsymbol{x}_t \in \mathbb{C}^{N_c \times 1}, \tag{1}$$

where $\mathbf{G}_i \in \mathbb{C}^{N \times L}$ is the time-varying UT-HRIS channel matrix at the i-th sub-frame, and $\boldsymbol{\Phi}_k \in \mathbb{C}^{Nc \times N}$ is the adjustable sensing phase-shift matrix, whose the (n_c, n)-th entry is given by $\sqrt{1 - \rho_{n,k}} e^{j\phi_{n_c,n,k}}$. Such a matrix corresponds to the k-th slice of the sensing tensor $\mathcal{T}_\Phi \in \mathbb{C}^{N_c \times N \times K}$. Meanwhile, the signal received by the M BS antennas, corresponding to the reflected portion, is given as

$$\boldsymbol{y}^{\mathrm{BS}}_{t,k,i} = \mathbf{H} \mathrm{diag}\left\{\boldsymbol{\psi}_k\right\} \mathbf{G}_i \mathbf{C}_k \boldsymbol{x}_t \in \mathbb{C}^{M \times 1}, \tag{2}$$

where $\mathbf{H} \in \mathbb{C}^{M \times N}$ is the quasi-static HRIS-BS channel matrix, and $\boldsymbol{\psi}_k = [\sqrt{\rho_{1,k}} e^{j\psi_{1,k}}, \cdots, \sqrt{\rho_{N,k}} e^{j\psi_{N,k}}]^{\mathrm{T}} \in \mathbb{C}^{N \times 1}$ is the reconfigurable reflecting phase-shift beam.

Collecting the received signals during T symbol periods of each k-th block, we get $\mathbf{Y}^{\mathrm{RC}}_{k,i} = [\boldsymbol{y}^{\mathrm{RC}}_{1,k,i}, \cdots, \boldsymbol{y}^{\mathrm{RC}}_{T,k,i}] \in \mathbb{C}^{N_c \times T}$ and $\mathbf{Y}^{\mathrm{BS}}_{k,i} = [\boldsymbol{y}^{\mathrm{BS}}_{1,k,i}, \cdots, \boldsymbol{y}^{\mathrm{BS}}_{T,k,i}] \in \mathbb{C}^{M \times T}$ on the HRIS and BS sides, respectively, given by

$$\mathbf{Y}^{\mathrm{RC}}_{k,i} = \boldsymbol{\Phi}_k \mathbf{G}_i \mathbf{C}_k \mathbf{X} \in \mathbb{C}^{N_c \times T} \tag{3}$$

and

$$\mathbf{Y}^{\mathrm{BS}}_{k,i} = \mathbf{H} \mathrm{diag}\left\{\boldsymbol{\psi}_k\right\} \mathbf{G}_i \mathbf{C}_k \mathbf{X} \in \mathbb{C}^{M \times T}, \tag{4}$$

where $\mathbf{X} \in \mathbb{C}^{R \times T}$ is the the symbol matrix.

III. Tensor Modeling and Closed-Form HRIS-KronF Receiver

Note that the sensing signal at (3) can be seen as a fourth-order tensor $\mathcal{Y}^{\mathrm{RC}} \in \mathbb{C}^{N_c \times T \times K \times I}$, where (3) denotes the (k, i)-th slice of the tensor $\mathcal{Y}^{\mathrm{RC}}$. Then, since that $\mathrm{vec}\{\mathbf{PQS}\} = (\mathbf{S}^{\mathrm{T}} \otimes \mathbf{P})\mathrm{vec}\{\mathbf{Q}\}$, its vectorized form is $\boldsymbol{y}^{\mathrm{RC}}_{k,i} = (\mathbf{X}^{\mathrm{T}} \otimes \mathbf{I}_{N_c})(\mathbf{C}^{\mathrm{T}}_k \otimes \boldsymbol{\Phi}_k)\boldsymbol{g}_i \in \mathbb{C}^{TN_c \times 1}$, where $\boldsymbol{g}_i = \mathrm{vec}\{\mathbf{G}_i\}$. By collecting the sensed signals from I sub-frames, we construct $\mathbf{Y}^{\mathrm{RC}}_k = [\boldsymbol{y}^{\mathrm{RC}}_{k,1}, \cdots, \boldsymbol{y}^{\mathrm{RC}}_{k,I}] \in \mathbb{C}^{TN_c \times I}$, given by

$$\mathbf{Y}^{\mathrm{RC}}_k = (\mathbf{X}^{\mathrm{T}} \otimes \mathbf{I}_{N_c})\mathbf{W}_k \mathbf{G}, \tag{5}$$

where the $\mathbf{W}_k = \mathbf{C}^{\mathrm{T}}_k \otimes \boldsymbol{\Phi}_k \in \mathbb{C}^{RN_c \times LN}$, and the matrix $\mathbf{G} = [\boldsymbol{g}_1, \cdots, \boldsymbol{g}_I] \in \mathbb{C}^{LN \times I}$ aggregates all the time-varying UT-HRIS channels among the I sub-frames. By applying the $\mathrm{vec}\{\cdot\}$ operator on (5), we get $\boldsymbol{y}^{\mathrm{RC}}_k \in \mathbb{C}^{ITN_c \times 1}$, given by

$$\boldsymbol{y}^{\mathrm{RC}}_k = (\mathbf{G}^{\mathrm{T}} \otimes \mathbf{X}^{\mathrm{T}} \otimes \mathbf{I}_{N_c})\boldsymbol{w}_k, \tag{6}$$

where $\boldsymbol{w}_k = \mathrm{vec}\{\mathbf{W}_k\} \in \mathbb{C}^{LNRN_c \times 1}$.

Now, leveraging the tensor unfolding concept, the matrix $\mathbf{Y}^{\mathrm{RC}}_k$ can be interpreted as an unfolding of a tensor $\mathcal{Y}^{\mathrm{RC}}_k \in \mathbb{C}^{N_c \times T \times I}$, which in turn corresponds to the k-th third order mode-3 tensor slice of $\mathcal{Y}^{\mathrm{RC}}$. In addition, the mode-1 and

mode-3 unfoldings of $\mathcal{Y}_k^{\mathrm{RC}}$ are denoted by $\big[\mathcal{Y}_k^{\mathrm{RC}}\big]_{(1)} \in \mathbb{C}^{N_c \times IT}$ and $\big[\mathcal{Y}_k^{\mathrm{RC}}\big]_{(3)} \in \mathbb{C}^{TN_c \times I}$, respectively. The equivalence between $\mathbf{Y}_k^{\mathrm{RC}}$ and the generalized/mode-n unfoldings of $\mathcal{Y}_k^{\mathrm{RC}}$ is $\mathbf{Y}_k^{\mathrm{RC}} = \big[\mathcal{Y}_k^{\mathrm{RC}}\big]_{([1,2],[3])} = \big[\mathcal{Y}_k^{\mathrm{RC}}\big]_{(3)}^{\mathrm{T}}$. In this way, $\boldsymbol{y}_k^{\mathrm{RC}}$ is related with the matrix unfoldings of $\mathcal{Y}_k^{\mathrm{RC}}$ as follows:

$$\boldsymbol{y}_k^{\mathrm{RC}} = \mathrm{vec}\big\{\big[\mathcal{Y}_k^{\mathrm{RC}}\big]_{(3)}^{\mathrm{T}}\big\} = \mathrm{vec}\big\{\big[\mathcal{Y}_k^{\mathrm{RC}}\big]_{(1)}\big\}. \tag{7}$$

Note that $\big[\mathcal{Y}_k^{\mathrm{RC}}\big]_{(1)}$ does not correspond to $\mathbf{Y}_k^{\mathrm{RC}}$, but its vectorized shape does. These equivalent vectorized forms are valuable for simplifying the derivation of this receiver. Thereafter, we construct the tensor $\mathcal{W}_k \in \mathbb{C}^{N_c \times R \times LN}$ by tensorizing the matrix $\mathbf{W}_k$ in such a way that it corresponds to the transpose mode-3 unfolding of $\mathcal{W}_k$. This can be realized by carrying out the reverse operation of the unfolding. The mode-1 and mode-3 unfoldings of $\mathcal{W}_k$ are denoted by $[\mathcal{W}_k]_{(1)} \in \mathbb{C}^{N_c \times LNR}$ and $[\mathcal{W}_k]_{(3)} \in \mathbb{C}^{LN \times RN_c}$, respectively. Similarly to $\mathbf{Y}_k^{\mathrm{RC}}$, the correspondence between $\mathbf{W}_k$ and the generalized/mode-n unfoldings of $\mathcal{W}_k$ is $\mathbf{W}_k = [\mathcal{W}_k]_{([1,2],[3])} = [\mathcal{W}_k]_{(3)}^{\mathrm{T}} \in \mathbb{C}^{RN_c \times LN}$. Likewise, its vectorized form $\boldsymbol{w}_k$ can be understood as

$$\boldsymbol{w}_k = \mathrm{vec}\big\{[\mathcal{W}_k]_{(3)}^{\mathrm{T}}\big\} = \mathrm{vec}\big\{[\mathcal{W}_k]_{(1)}\big\} \in \mathbb{C}^{LNRN_c \times 1}. \tag{8}$$

Exploiting (7) and (8), while taking into account the mode-1 unfolding, we can recast (6) as

$$\mathrm{vec}\big\{\big[\mathcal{Y}_k^{\mathrm{RC}}\big]_{(1)}\big\} = (\mathbf{Z}^{\mathrm{T}} \otimes \mathbf{I}_{N_c})\mathrm{vec}\big\{[\mathcal{W}_k]_{(1)}\big\}, \tag{9}$$

where $\mathbf{Z} = \mathbf{G} \otimes \mathbf{X} \in \mathbb{C}^{LNR \times IT}$. Doing $\big[\mathcal{Y}_k^{\mathrm{RC}}\big]_{(1)} = \mathrm{unvec}_{N_c \times IT}\big\{\mathrm{vec}\big\{\big[\mathcal{Y}_k^{\mathrm{RC}}\big]_{(1)}\big\}\big\}$, we get

$$\big[\mathcal{Y}_k^{\mathrm{RC}}\big]_{(1)} = [\mathcal{W}_k]_{(1)}\,\mathbf{Z}. \tag{10}$$

Finally, by gathering all the K unfolding-like tensor slices $[\mathcal{Y}_k^{\mathrm{RC}}]_{(1)}$, we construct the generalized unfolding $\big[\mathcal{Y}^{\mathrm{RC}}\big]_{([1,3],[2,4])} \in \mathbb{C}^{KN_c \times IT}$, i.e, $\big[\mathcal{Y}^{\mathrm{RC}}\big]_{([1,3],[2,4])} = \big[[\mathcal{Y}_1^{\mathrm{RC}}]_{(1)}^{\mathrm{T}}, \cdots, [\mathcal{Y}_K^{\mathrm{RC}}]_{(1)}^{\mathrm{T}}\big]^{\mathrm{T}}$, given by

$$\big[\mathcal{Y}^{\mathrm{RC}}\big]_{([1,3],[2,4])} = \big[\mathcal{W}\big]_{([1,3],[2,4])}\mathbf{Z}, \tag{11}$$

where $[\mathcal{W}]_{([1,3],[2,4])} \in \mathbb{C}^{KN_c \times LNR}$ is a generalized unfolding of the 4-th order tensor $\mathcal{W} \in \mathbb{C}^{N_c \times R \times K \times LN}$ constructed from collecting all the K unfolding-like tensor slices $[\mathcal{W}_k]_{(1)}$, i.e., $[\mathcal{W}]_{([1,3],[2,4])} = \big[[\mathcal{W}_1]_{(1)}^{\mathrm{T}}, \cdots, [\mathcal{W}_K]_{(1)}^{\mathrm{T}}\big]^{\mathrm{T}}$. From (11), we get an estimate of the composite matrix $\mathbf{Z}$ by solving the problem

$$\hat{\mathbf{Z}} = \arg\min_{\mathbf{Z}} \big|\big|\big[\mathcal{Y}^{\mathrm{RC}}\big]_{([1,3],[2,4])} - \big[\mathcal{W}\big]_{([1,3],[2,4])}\mathbf{Z}\big|\big|_{\mathrm{F}}^2 \tag{12}$$

whose analytical solution is

$$\hat{\mathbf{Z}} = \big[\mathcal{W}\big]_{([1,3],[2,4])}^{\dagger}\big[\mathcal{Y}^{\mathrm{RC}}\big]_{([1,3],[2,4])}. \tag{13}$$

The next step involves employing the LS-Kronecker Factorization (KronF) algorithm on $\hat{\mathbf{Z}}$, which generates a rank-1 matrix $\bar{\mathbf{Z}} \in \mathbb{C}^{TR \times ILN}$ by rearranging it (see details in [19]). The best rank-1 approximation of $\hat{\mathbf{G}}$ and $\hat{\mathbf{X}}$ is obtained from the truncated singular value decomposition (SVD) of $\bar{\mathbf{Z}}$. Algorithm 1 briefs the key steps of the HRIS-KronF receiver.

Algorithm 1: HRIS-KronF receiver

1. Using (13), find a LS estimate of $\hat{\mathbf{Z}}$;
2. Construct $\bar{\mathbf{Z}}$ by rearranging $\hat{\mathbf{Z}}$;
3. Compute $[\boldsymbol{u}_1, \sigma_1, \boldsymbol{v}_1] \longleftarrow$ truncated-SVD($\bar{\mathbf{Z}}$);
4. Reconstruct $\hat{\mathbf{X}}$ and $\hat{\mathbf{G}}$:
   $\hat{\mathbf{G}} \leftarrow \mathrm{unvec}_{LN \times I}\{\sqrt{\sigma_1}\boldsymbol{v}_1^*\}$, $\hat{\mathbf{X}} \leftarrow \mathrm{unvec}_{R \times T}\{\sqrt{\sigma_1}\boldsymbol{u}_1\}$;
5. Remove scaling ambiguities.

IV. Least-Squares HRIS-BS Channel Estimation

At the BS side, we collect the matrices $\mathbf{Y}_{k,i}^{\mathrm{BS}}$ during the K blocks associated with the i-th sub-frame by defining $\mathbf{Y}_i^{\mathrm{BS}} = \big[\mathbf{Y}_{1,i}^{\mathrm{BS}}, \cdots, \mathbf{Y}_{K,i}^{\mathrm{BS}}\big] \in \mathbb{C}^{M \times KT}$, given by

$$\mathbf{Y}_i^{\mathrm{BS}} = \mathbf{H}\mathbf{F}_i(\mathbf{I}_K \otimes \mathbf{X}), \tag{14}$$

where

$$\mathbf{F}_i = [\mathrm{diag}\{\boldsymbol{\psi}_1\}\mathbf{G}_i\mathbf{C}_1, \cdots, \mathrm{diag}\{\boldsymbol{\psi}_K\}\mathbf{G}_i\mathbf{C}_K] \in \mathbb{C}^{N \times KL}. \tag{15}$$

To capture the variation of the UT-HRIS channel across the I subframes, we stack column-wise the received signals $\mathbf{Y}_i^{\mathrm{BS}}$ during the I sub-frames by defining $\mathbf{Y}^{\mathrm{BS}} = \big[\mathbf{Y}_1^{\mathrm{BS}}, \cdots, \mathbf{Y}_I^{\mathrm{BS}}\big] \in \mathbb{C}^{M \times IKT}$ and get

$$\mathbf{Y}^{\mathrm{BS}} = \mathbf{H}\mathbf{F}(\mathbf{I}_{IK} \otimes \mathbf{X}), \tag{16}$$

where $\mathbf{F} = [\mathbf{F}_1, \cdots, \mathbf{F}_I] \in \mathbb{C}^{N \times IKL}$ encapsulates all the I states of the time-varying UT-HRIS channel. To estimate the HRIS-BS channel, we consider the following LS criterion

$$\hat{\mathbf{H}} = \arg\min_{\mathbf{H}} \big|\big|\mathbf{Y}^{\mathrm{BS}} - \mathbf{H}\mathbf{F}(\mathbf{I}_{IK} \otimes \mathbf{X})\big|\big|_{\mathrm{F}}^2. \tag{17}$$

Recall that the task of estimating $\mathbf{G} \in \mathbb{C}^{LN \times I}$ and $\mathbf{X} \in \mathbb{C}^{R \times T}$ is conducted by the HRIS controller, and these estimates are conveyed to the BS *via* a feedback control link. The matrices $\hat{\mathbf{G}}_i$ ($i = 1, \cdots, I$) are formed by reshaping the columns of $\hat{\mathbf{G}}$, i.e. $\hat{\mathbf{G}}_i = \mathrm{unvec}_{N \times L}\{\hat{\boldsymbol{g}}_i\}$. An LS estimate of the HRIS-BS channel is obtained by solving (17), where $\mathbf{F}$ is constructed from the estimates of the UT-HRIS channels according to (15) and $\mathbf{X}$ are replaced by their estimates obtained at the HRIS (c.f. step 4 of Algorithm 1), which gives

$$\hat{\mathbf{H}} = \mathbf{Y}^{\mathrm{BS}}\big[\bar{\mathbf{F}}(\mathbf{I}_{IK} \otimes \hat{\mathbf{X}})\big]^{\dagger}. \tag{18}$$

Note that assuming that $\bar{\mathbf{F}}$ and $\hat{\mathbf{X}}$ are full row-rank, we can simplify the computation of the pseudo-inverse in the previous equation, yielding $\hat{\mathbf{H}} = \mathbf{Y}^{\mathrm{BS}}(\mathbf{I}_{IK} \otimes \hat{\mathbf{X}}^{\dagger})\bar{\mathbf{F}}^{\dagger}$.

V. Scaling Ambiguities, Computational Complexity, and Identifiability

At the HRIS side, after applying the rank-one approximations to $\mathbf{G}$ and $\mathbf{X}$ through truncated SVDs using the KronF algorithm, the estimates are unique except for a scaling factor such that $\mathbf{G} = \alpha\hat{\mathbf{G}}$ and $\mathbf{X} = (1/\alpha)\hat{\mathbf{X}}$. Such a scaling factor can be eliminated by assuming the knowledge of one symbol in $\mathbf{X}$ at the receiver. The computational complexity of our proposed receiver involves a complexity of $\mathcal{O}(L^2N^2R^2KN_c)$ for the inversion of $\big[\mathcal{W}\big]_{([1,3],[2,4])}$, followed by $\mathcal{O}(LNRIT)$

to compute the truncated-SVD of the rank-1 matrix $\bar{\mathbf{Z}}$ within the KronF algorithm. Note that the complexity of the inverse can be reduced by properly designing $\mathcal{T}_\Phi$ and $\mathcal{C}$ such that $[\mathcal{W}]_{([1,3],[2,4])}$ is column-orthogonal.

VI. Results and Discussion

In this section, we evaluate the performance of our proposed semi-blind receiver in terms of symbol error rate (SER) and normalized mean squared error (NMSE) of the estimated channels, which is defined as $\text{NMSE}(\mathbf{P}) = \left|\left|\mathbf{P}-\hat{\mathbf{P}}\right|\right|_{\text{F}}^2 / \left|\left|\mathbf{P}\right|\right|_{\text{F}}^2$ after 10^3 Monte Carlos runs, in which $\mathbf{P}$ is $\mathbf{G}$ or $\mathbf{H}$. We adopt the parameter set $\{M, N, N_c, R, L, T, K\} = \{8, 32, 4, 2, 2, 4, 32\}$ and 64-QAM as modulation scheme for data symbol matrix. Further, we consider a loss of -20dB reference distance of $1m$. Our setup includes UT-HRIS and HRIS-BS links with $20m$ and $50m$ distances, respectively. In the simulations, we assume a Rayleigh fading channel and that both HRIS and BS share the same noise power level generated based on the transmit SNR (t-SNR) values.

Figure 2 shows the results of SER and NMSE of the time-varying UT-HRIS channel at the HRIS controller under variations of the power splitting parameter. We set t-SNR $= 25$dB and $I = 2$. Both of them increase as ρ increases since each meta-atom's enhanced reflection capability reduces its sensing capacity, and vice-versa. This analysis reveals the symbol detection behavior when ρ is changed, and such findings align with predictions in [23] regarding the NMSE of $\mathbf{G}$. Given that CE at the HRIS side is less influenced by path loss than the estimates obtained at the BS, we set $\rho = 90\%$ in our simulations. This configuration ensures that estimating $\mathbf{X}$ and the time-varying channels $\mathbf{G}_i$ remain effective despite the reduced sensing capability. This means the lower path loss of the UT-HRIS link compensates estimations at the HRIS, while at BS, it is by the higher value of ρ.

Figure 3 depicts the NMSE of the individual time-varying UT-HRIS and the HRIS-BS channels for different sub-frame lengths as a function of the t-SNR. Firstly, we assess the UT-HRIS CE performance at the HRIS controller. Regarding NMSE results of the composite channel matrix $\mathbf{G}$, which encompass all versions of $\mathbf{G}_i$. Such results demonstrate the robust capability of the HRIS to perform CE. Furthermore, the HRIS's strategic positioning corroborates its performance since it suffers less path loss than the received signal at the BS even under $\rho = 90\%$ (only 10% of meta-atom's sensing capability). Besides, we highlight the robustness of our proposed closed-form semi-blind receiver in capturing all variations of the UT-HRIS channels. At the end of the time protocol, the HRIS controller feeds $\hat{\mathbf{G}}$ back to the BS *via* control link. Using this information, the BS estimates $\mathbf{H}$. Even though carrying estimation errors, leveraging $\hat{\mathbf{G}}$ to estimate $\mathbf{H}$ is a good choice by considering a high transmit SNR regime, leaving the estimation performance depending mainly on the path loss involved in the HRIS-BS link.

Next, we evaluate the symbol detection performance of the proposed semi-blind receiver. Figure 4 exhibits SER results as a function of the transmit SNR. The results show a remarkable performance even in the low SNR regime. Note that the range of the SER analysis is anticipated in relation to the NMSE

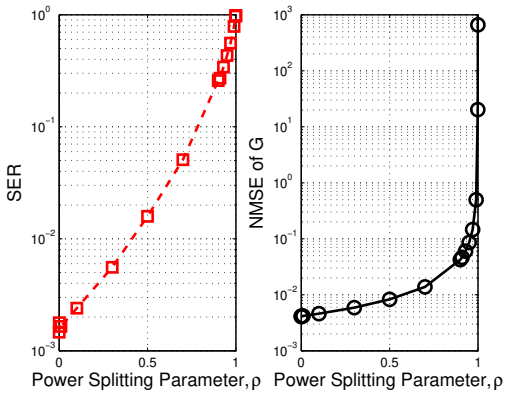

Fig. 2. SER and NMSE of UT-HRIS channel vs. ρ.

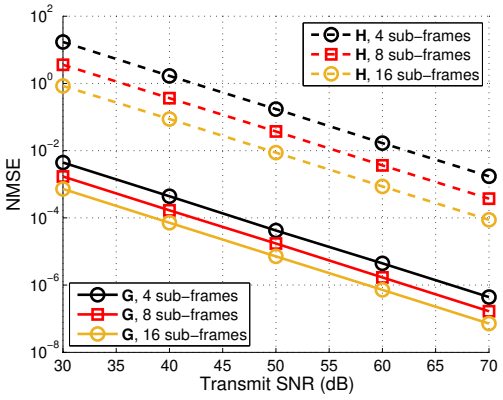

Fig. 3. NMSE of the channels vs. transmit SNR.

ones. These results underscore the HRIS controller's impressive precision in joint symbol and CE. In only CE scope, such precision was already predicted in [23]. Moreover, the semi-blind approach allows the UT to transmit data symbols, extending beyond pilot sequences within the same blocks.

As we can see from Figs. 3, and 4, the performance of the proposed semi-blind estimation scheme is enhanced when the number I of collected sub-frames is increased since the HRIS captures more UT-HRIS channel variations, resulting in an increased receiver diversity. For instance, by increasing $I = 4$ to $I = 16$, the algorithm exhibits an SNR gain of nearly 10 dB. Note, however, that higher accuracy of the channel estimates obtained by increasing the number of processed sub-frames comes with a reduction in the transmission rate since the symbol matrix $\mathbf{X}$ is retransmitted KT times for each i-th sub-frame. Figure 5 takes a closer look at this point by plotting the NMSE curves related to the number of sub-frames.

VII. Conclusions

This work has addressed semi-blind channel and symbol estimation for HRIS-assisted communications in a scenario with a certain level of user mobility. It demonstrates the effectiveness of the proposed semi-blind receiver in estimating the time-varying UT-HRIS channel and the HRIS-BS one with limited sensing capability at the HRIS. We analyzed the trade-off between reflection and sensing capacity, highlighting the

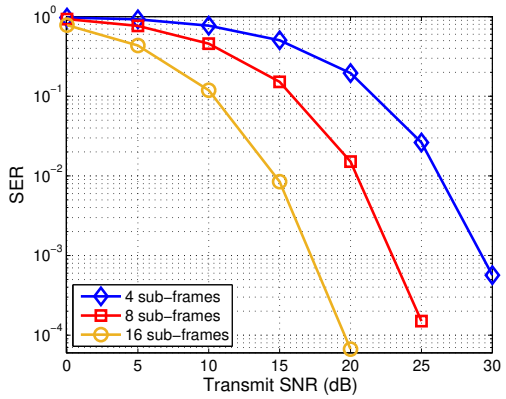

Fig. 4. SER vs. transmit SNR.

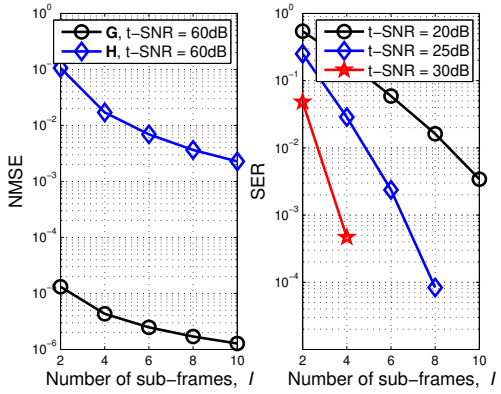

Fig. 5. NMSE of the channels vs. number of sub-frames.

performance of the estimation task at the HRIS controller, whose results align with previous predictions in the literature. Our results indicate that allowing the HRIS to estimate both the uplink channel and user symbols is a viable strategy, particularly in high SNR regimes. Furthermore, the symbol detection performance underscores the HRIS controller's precision in joint symbol and CE, even under challenging conditions. The observed performance improves as more sub-frames are processed at the HRIS, highlighting the diversity gains achievable through the proposed approach. However, these gains come at the cost of reduced transmission rates, which must be considered when designing practical systems. Perspectives include studying methods for reducing the feedback between the HRIS and the BS, which is necessary to estimate the HRIS-BS channel at the BS. Future work should also consider more realistic (physical) channel models and an extension of our proposed semi-blind receiver to multi-user systems.

REFERENCES

[1] E. Basar, "Reconfigurable intelligent surface-based index modulation: A new beyond MIMO paradigm for 6G," *IEEE Transactions on Communications*, vol. 68, no. 5, pp. 3187–3196, 2020.

[2] Q. Wu and R. Zhang, "Towards smart and reconfigurable environment: Intelligent reflecting surface aided wireless network," *IEEE communications magazine*, vol. 58, no. 1, pp. 106–112, 2020.

[3] J. Chen, Y.-C. Liang, H. V. Cheng, and W. Yu, "Channel estimation for reconfigurable intelligent surface aided multi-user mmWave MIMO systems," *IEEE Trans. Wireless Commun.*, vol. 22, no. 10, pp. 6853–6869, 2023.

[4] A. L. Swindlehurst, G. Zhou, R. Liu, C. Pan, and M. Li, "Channel estimation with reconfigurable intelligent surfaces — a general framework," *Proceedings of the IEEE*, vol. 110, no. 9, pp. 1312–1338, 2022.

[5] Q. Wu and R. Zhang, "Beamforming optimization for wireless network aided by intelligent reflecting surface with discrete phase shifts," *IEEE Trans. Commun.*, vol. 68, no. 3, pp. 1838–1851, 2020.

[6] J. Choi and J. H. Cho, "A joint optimization of pilot and phase shifts in uplink channel estimation for hybrid ris-aided multi-user communication systems," *IEEE Transactions on Vehicular Technology*, 2023.

[7] S. E. Zegrar, L. Afeef, and H. Arslan, "A general framework for RIS-aided mmWave communication networks: Channel estimation and mobile user tracking," *arXiv preprint arXiv:2009.01180*, 2020.

[8] Y. Sun, K. An, Y. Zhu, G. Zheng, K.-K. Wong, S. Chatzinotas, D. W. K. Ng, and D. Guan, "Energy-efficient hybrid beamforming for multilayer ris-assisted secure integrated terrestrial-aerial networks," *IEEE Trans. Commun.*, vol. 70, no. 6, pp. 4189–4210, 2022.

[9] J. Zhu, K. Liu, Z. Wan, L. Dai, T. J. Cui, and H. V. Poor, "Sensing RISs: Enabling dimension-independent CSI acquisition for beamforming," *IEEE Trans. Inf. Theory*, vol. 69, no. 6, pp. 3795–3813, 2023.

[10] A. Taha, M. Alrabeiah, and A. Alkhateeb, "Enabling large intelligent surfaces with compressive sensing and deep learning," *IEEE access*, vol. 9, pp. 44 304–44 321, 2021.

[11] I. Alamzadeh, G. C. Alexandropoulos, N. Shlezinger, and M. F. Imani, "A reconfigurable intelligent surface with integrated sensing capability," *Scientific reports*, vol. 11, no. 1, p. 20737, 2021.

[12] G. C. Alexandropoulos, N. Shlezinger, I. Alamzadeh, M. F. Imani, H. Zhang, and Y. C. Eldar, "Hybrid reconfigurable intelligent metasurfaces: Enabling simultaneous tunable reflections and sensing for 6G wireless communications," *IEEE Vehicular Technology Magazine*, vol. 19, no. 1, pp. 75–84, 2024.

[13] E. Basar, G. C. Alexandropoulos, Y. Liu, Q. Wu, S. Jin, C. Yuen, O. A. Dobre, and R. Schober, "Reconfigurable intelligent surfaces for 6G: Emerging hardware architectures, applications, and open challenges," *arXiv preprint arXiv:2312.16874*, 2023.

[14] N. D. Sidiropoulos, G. B. Giannakis, and R. Bro, "Blind PARAFAC receivers for DS-CDMA systems," *IEEE Trans. Signal Process.*, vol. 48, no. 3, pp. 810–823, 2000.

[15] G. Favier and A. L. F. de Almeida, "Overview of constrained parafac models," *EURASIP J. Adv. Signal Process.*, vol. 2014, no. 142, pp. 1–25, Sep. 2014.

[16] ——, "Tensor space-time-frequency coding with semi-blind receivers for MIMO wireless communication systems," *IEEE Trans. Signal Process.*, vol. 62, no. 22, pp. 5987–6002, 11 2014.

[17] B. Sokal, P. R. Gomes, A. L. F. de Almeida, and M. Haardt, "Tensor-based receiver for joint channel, data, and phase-noise estimation in MIMO-OFDM systems," *IEEE J. Sel. Topics Signal Process.*, vol. 15, no. 3, pp. 803–815, 2021.

[18] G. T. de Araújo, A. L. F. de Almeida, and R. Boyer, "Channel estimation for intelligent reflecting surface assisted MIMO systems: A tensor modeling approach," *IEEE J. Sel. Topic in Signal Process.*, vol. 15, no. 3, pp. 789–802, 2021.

[19] G. T. de Araújo, P. R. Gomes, A. L. F. de Almeida, G. Fodor, and B. Makki, "Semi-blind joint channel and symbol estimation in IRS-assisted multiuser MIMO networks," *IEEE Wireless Communications Letters*, vol. 11, no. 7, pp. 1553–1557, 2022.

[20] G. T. de Araújo, A. L. F. de Almeida, R. Boyer, and G. Fodor, "Semi-blind joint channel and symbol estimation for IRS-assisted MIMO systems," *IEEE Trans. on Signal Process.*, vol. 71, pp. 1184–1199, 2023.

[21] P. R. Gomes, G. T. de Araújo, B. Sokal, A. L. F. de Almeida, B. Makki, and G. Fodor, "Channel estimation in RIS-assisted MIMO systems operating under imperfections," *IEEE Trans. Veh. Technol.*, 2023.

[22] F. Roemer, C. Schroeter, and M. Haardt, "A semi-algebraic framework for approximate CP decompositions via joint matrix diagonalization and generalized unfoldings," in *In Proc. IEEE ASILOMAR Conf. Signals, Syst., Comput.,*. IEEE, 2012, pp. 2023–2027.

[23] H. Zhang, N. Shlezinger, G. C. Alexandropoulos, A. Shultzman, I. Alamzadeh, M. F. Imani, and Y. C. Eldar, "Channel estimation with hybrid reconfigurable intelligent metasurfaces," *IEEE transactions on communications*, vol. 71, no. 4, pp. 2441–2456, 2023.

[24] X. Hu, R. Zhang, and C. Zhong, "Semi-passive elements assisted channel estimation for intelligent reflecting surface-aided communications," *IEEE Trans. Wireless Commun.*, vol. 21, no. 2, pp. 1132–1142, 2022.